Virologica Sinica 41 (2026) 612–623

Contents lists available at ScienceDirect

Virologica Sinica

journal homepage: www.keaipublishing.com/en/journals/virologica-sinica
www.virosin.org

Research Article

RNF26 bridges ER stress and autophagy in the clearance of MERS envelope protein

Ziyue Li [a,b,c,1], Yang Wang [d,1], Jingbo Qie [e], Shuangqu Li [b], Zhaobing Gao [a,b,c], Hin Chu [d,f,g,*], Bingqing Xia [b,c,*]

[a] School of Chinese Materia Medica, Nanjing University of Chinese Medicine, Nanjing 210046, China
[b] CAS Key Laboratory of Receptor Research, State Key Laboratory of Drug Research, Shanghai Institute of Materia Medica, Chinese Academy of Sciences, Shanghai 201203, China
[c] University of Chinese Academy of Sciences, Beijing 100049, China
[d] State Key Laboratory of Emerging Infectious Diseases, Department of Microbiology, School of Clinical Medicine, Li Ka Shing Faculty of Medicine, The University of Hong Kong, and Pandemics Research Alliance Unit at the University of Hong Kong, Hong Kong Special Administrative Region, China
[e] Shanghai Fifth People's Hospital and Institutes of Biomedical Sciences, Fudan University, Shanghai 200032, China
[f] Centre for Virology, Vaccinology and Therapeutics, Hong Kong Science and Technology Park, Hong Kong Special Administrative Region, China
[g] Materials Innovation Institute for Life Sciences and Energy (MILES), HKU-SIRI, Shenzhen 518000, China

ARTICLE INFO

Keywords:
Coronavirus envelope (E) proteins
Autophagy
Host-virus interaction
Cellular stress response
Pathogenicity

ABSTRACT

Coronavirus envelope (E) proteins are small, highly conserved viroporins essential for virion assembly and pathogenicity. Despite extensive characterization of their ion channel activity, how host cells sense and dispose of excessive viral membrane proteins remains poorly understood. Here we show that expression of the MERS-CoV E protein triggers pronounced ER stress and autophagy activation in human cells. The E protein is selectively degraded through an RNF26-dependent autophagy-lysosome pathway, and inhibition of autophagy or loss of RNF26 function leads to E accumulation and sustained unfolded protein response. Mechanistically, RNF26, an ER-anchored E3 ubiquitin ligase, promotes RING-dependent clearance of the viral protein through an ER protein quality control-associated pathway linked to autophagy and ER stress adaptation. Disruption of this process establishes a self-amplifying ER stress–autophagy feedback loop that exacerbates proteotoxicity. These findings define a membrane homeostatic conflict between viral viroporins and the host defense machinery, and identify RNF26 as a potential therapeutic target for mitigating viroporin-induced cytotoxicity through host-directed intervention.

INTRODUCTION

Coronavirus envelope proteins (E) are short, highly conserved membrane proteins typically composed of 76–109 amino acids and are present in coronaviruses (Schoeman and Fielding, 2019; Minigulov et al., 2024). The E protein plays an essential role in viral replication, assembly, and pathogenicity. Structural and functional studies have shown that E forms ion channels (viroporins) that modulate membrane potential and host signaling (Liu et al., 2024; Volovik et al., 2024; Sučec et al., 2025). For example, the SARS-CoV E protein mediates Ca^{2+} influx and activates the NLRP3 inflammasome, leading to IL-1β release and inflammatory responses (Nieto-Torres et al., 2015). Despite these advances, the precise molecular function of E within host cells remains poorly understood. Although E proteins are structurally conserved across coronaviruses, their roles in regulating cellular fate, maintaining membrane homeostasis, and contributing to viral pathogenicity vary substantially. A key unresolved question is how host cells manage the heavy burden of these abundant small membrane proteins, and whether E proteins themselves actively modulate host membrane homeostasis through specific cellular pathways.

* Corresponding authors.
E-mail addresses: xiabingqing@simm.ac.cn (B. Xia), hinchu@hku.hk (H. Chu).
Peer review under the responsibility of editorial board of *Virologica Sinica*.
[1] Ziyue Li and Yang Wang contributed equally to this work.

https://doi.org/10.1016/j.virs.2026.06.005
Received 5 December 2025; Accepted 5 June 2026
Available online 9 June 2026

Coronavirus replication and assembly are tightly coupled to the endoplasmic reticulum (ER) and its derived membrane networks (Klein et al., 2020; Williams et al., 2023). During infection, viral replication complexes remodel the ER into double-membrane vesicles (DMVs) that serve as platforms for RNA synthesis and protein translation (Wolff et al., 2020; Wang et al., 2025). This extensive membrane biogenesis imposes a substantial burden on the ER folding and processing machinery, activating the unfolded protein response (UPR) to restore homeostasis (Siu et al., 2014; Echavarría-Consuegra et al., 2021). When the stress persists or viral membrane proteins accumulate excessively, ER quality control mechanisms become overloaded, leading to protein misfolding, Ca^{2+} imbalance, and membrane remodeling (Sala et al., 2025). Such disruption of membrane homeostasis not only supports viral assembly but also drives cellular injury. Positioned at the ER-Golgi intermediate compartment (ERGIC), the E protein resides at the core of this membrane conflict (Li et al., 2024; Li et al., 2025). Excessive E expression alters membrane permeability, perturbs ion homeostasis, and triggers ER stress, suggesting that it may act both as a structural component for virion morphogenesis and as a potent inducer of host membrane stress.

When ER stress cannot be fully resolved by the UPR, cells engage autophagy as a secondary defense mechanism to remove damaged membranes and misfolded proteins (Rashid et al., 2015). Autophagy selectively engulfs abnormal structures into autophagosomes and delivers them to lysosomes for degradation, thereby restoring proteostasis. In addition, increasing evidence further reveals a tight coupling between ubiquitination and autophagy in determining the fate of viral proteins. Several viral structural proteins, such as HIV-1 Gag (Castro-Gonzalez et al., 2021) and coxsackievirus VP1 (Mohamud et al., 2019), undergo K63-linked ubiquitination and are subsequently cleared via p62-or NDP52-mediated autophagy, underscoring the central role of the "ubiquitin-autophagy axis" in antiviral protein quality control. Yet, for coronaviruses, whether structural proteins, particularly E, can be recognized and degraded through this pathway remains unclear. Previous studies on MERS-CoV have largely focused on nonstructural and accessory proteins in the regulation of autophagy. For example, nsp1 induces autophagy initiation but blocks flux (Feng et al., 2022). ORF4b modulates p62 levels and autophagy gene expression (Bello-Perez et al., 2022) and ORF5 overexpression causes LC3-II and p62 accumulation (Gassen et al., 2019), indicative of impaired autophagosome turnover. By contrast, the role of the E protein, an integral component directly involved in viral assembly, remains undefined.

In this study, we investigated the molecular and cellular functions of the MERS-CoV envelope protein (MERS-E). We found that MERS-E expression markedly reduces cell viability and robustly activates autophagy, suggesting a disturbance of host proteostasis. Mechanistic analyses revealed that E not only triggers autophagy but also engages ER stress and degradative signaling. Through integrated molecular and cellular approaches, we delineate how E perturbs the balance between membrane homeostasis and degradation, establishing an ER stress-autophagy feedback loop. These findings provide a mechanistic framework for understanding how coronavirus structural proteins reshape host cell pathology and highlight new perspectives for targeting virus-host homeostatic interactions.

RESULTS

MERS-E expression reduces cell viability and induces autophagy

To assess the cellular effects of MERS-CoV envelope protein (MERS-E), we expressed MERS-E in HEK293T (human embryonic kidney), H292 (human lung mucoepidermoid carcinoma), A549 (human lung adenocarcinoma) and 16HBE (human bronchial epithelial) cells transiently. Overexpression of MERS-E markedly reduced cell proliferation and viability compared with vector controls (Fig. 1A), indicating that the MERS-E protein exerts cytotoxic effects. Consistent with this, flow cytometric analysis revealed a significant increase in propidium iodide (PI)-positive cells following MERS-E expression (Fig. 1B), suggesting compromised cell membrane integrity in a subset of stressed cells. To determine whether MERS-E–induced loss of viability is associated with specific cell death pathways, we examined molecular markers of apoptosis, pyroptosis, necroptosis, and autophagy. Immunoblot analysis showed no significant activation of apoptotic or necroptotic markers, such as caspase-3, caspase-7, MLKL, and GSDME et al., whereas autophagy-related proteins were prominently altered. Specifically, MERS-E expression markedly increased the phosphatidylethanolamine-conjugated form of LC3, as evidenced by an elevated LC3-II/LC3-I ratio (Fig. 1C). As a positive control, TSZ-treated HT29 cells were used to confirm the validity of the antibodies for detecting RIPK3, p-RIPK3, MLKL, and p-MLKL (Supplementary Fig. S1A). Further analyses of canonical autophagy markers revealed that MERS-E overexpression increased LC3-II accumulation and reduced the autophagic substrate p62, along with upregulation of Beclin-1, indicating enhanced autophagic flux (Fig. 1D). Consistent with these biochemical findings, transmission electron microscopy (TEM) revealed an increased number of double-membrane autophagosomes in MERS-E–expressing cells (Fig. 1E). Pharmacological inhibition of autophagy further supported that MERS-E is subject to autophagic degradation. Blocking autophagy initiation with 3-methyladenine (3-MA) or by interfering with autophagosome–lysosome fusion and lysosomal acidification using chloroquine (CQ) or bafilomycin A1 (BafA1) led to a marked accumulation of MERS-E protein compared with untreated cells, suggesting that MERS-E is degraded through the autophagy–lysosome pathway (Fig. 1F, Supplementary Fig. S1B–C). Cells were treated with pharmacological inhibitors of autophagy to assess whether autophagy-related processes contribute to MERS-E–induced loss of viability. CCK-8 assays showed that BafA1 significantly restored cell viability, whereas 3-MA and CQ showed only a modest recovery trend. These results suggest that autophagy lysosome-associated processes contribute, at least in part, to MERS-E-induced loss of viability (Supplementary Fig. S1D).

Proteomic profiling reveals coordinated activation of autophagy and ubiquitin–proteasome pathways by MERS-E

To elucidate the molecular mechanisms underlying MERS-E-induced autophagy, we performed quantitative proteomic analysis of cells overexpressing MERS-E compared with vector controls. Gene set variation analysis (GSVA) based on the KEGG database revealed widespread alterations in cellular homeostatic pathways upon MERS-E expression (Fig. 2A–C, Supplementary Fig. S2A–B). Among these, the "Autophagy–animal" and "Ubiquitin mediated proteolysis" pathways were prominently enriched, indicating that MERS-E triggers a coordinated activation of protein degradation systems. Gene set enrichment analysis (GSEA) confirmed these findings and further highlighted upregulation of complement and Toll-like receptor signaling, consistent with an inflammatory stress response. To identify key regulatory factors bridging the autophagy and ubiquitin pathways, we integrated the proteomic dataset with curated autophagy- and ubiquitin-related protein databases. Manual annotation of 111 differentially expressed proteins yielded 21 candidates involved in both processes, among which three proteins (ATG12, RNF26, and UBB) acted as dual regulators rather than simple substrates or degradation targets (Fig. 2D). These intersectional regulators are positioned at the nexus of ubiquitin signaling and autophagic flux, suggesting their potential role in modulating the fate of MERS-E. We next prioritized these candidates based on their function (Fig. 2E). UBB represents the ubiquitin backbone itself, whose perturbation would cause global proteostasis disruption (Han et al., 2021; Wagh et al., 2023), whereas ATG12 is indispensable for autophagosome formation and does not specifically regulate substrate selectivity (Otomo et al., 2013; Walczak and Martens, 2013). In contrast, RNF26, an endoplasmic reticulum-anchored E3 ubiquitin ligase recently implicated in selective autophagy and innate immune signaling, presents a

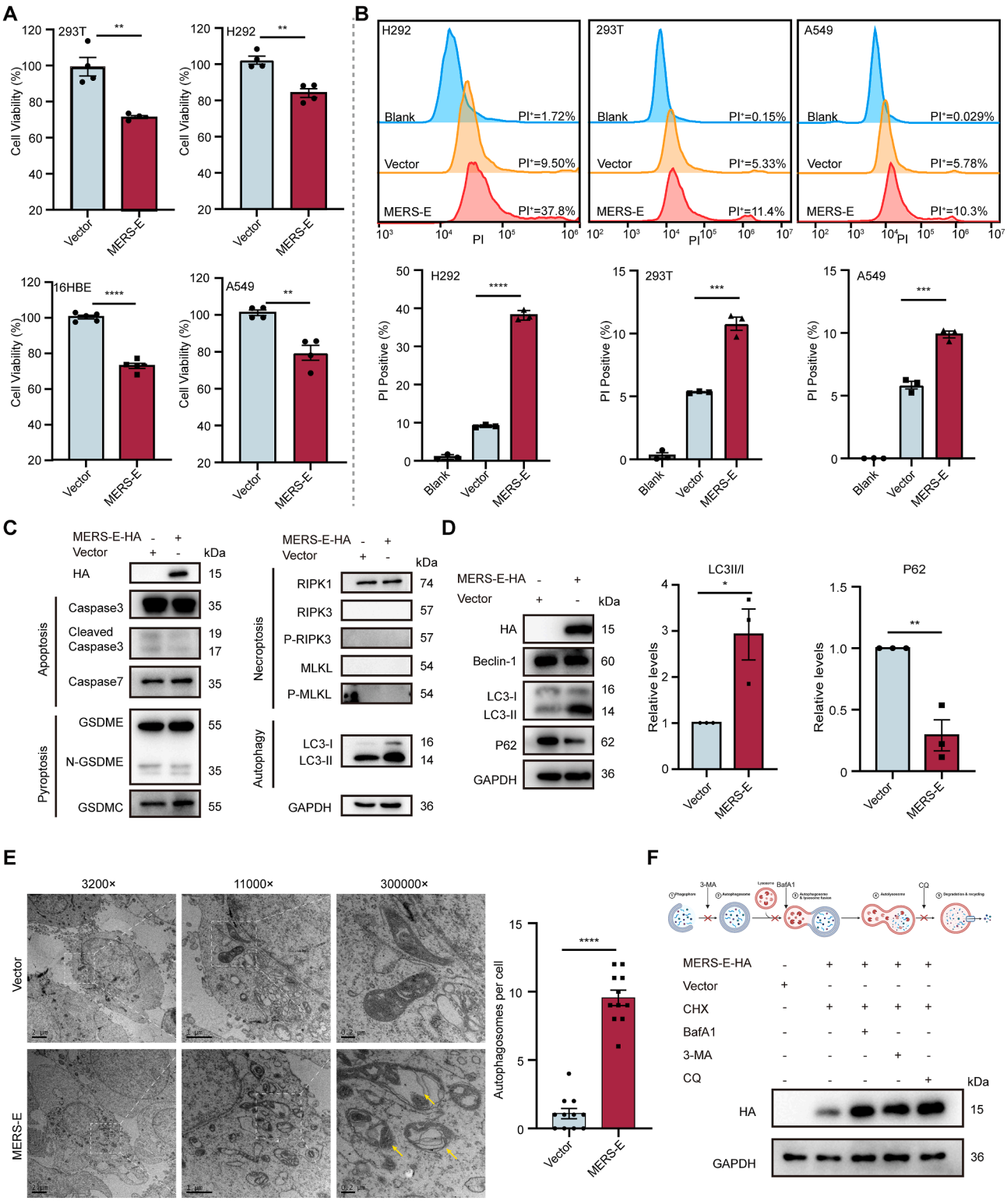

Fig. 1. MERS-E expression reduces cell viability and induces autophagy. **A** Cell viability of HEK293T, H292, 16HBE, and A549 cells after transfection with MERS-E or empty vector for 24 h. **B** Flow cytometry histograms of PI staining (top) and statistical analysis of PI-positive cells (bottom) in H292, HEK293T, and A549 cells expressing MERS-E-HA or empty vector for 24 h. **C** H292 cells were transfected with empty vector or MERS-E-HA for 24 h and analyzed by Western blotting with the indicated antibodies. **D** H292 cells were transfected with empty vector or MERS-E-HA for 24 h and analyzed by Western blot with the indicated antibodies (left). Quantification of LC3-II/I and p62 expression (right) by densitometric analysis using ImageJ ($N = 3$). **E** TEM images of HEK293T cells transfected with MERS-E-HA or empty vector (left). Yellow arrows indicate autophagic structures. Quantification of autophagosome numbers per cell (right; $N = 11$). Scale bars, 2 μm (left), 1 μm (middle), and 0.2 μm (right). **F** Schematic illustration of the autophagy process and the corresponding inhibitory stages of each autophagy inhibitor (top). HEK293T cells were transfected with empty vector or MERS-E-HA plasmid for 24 h and subsequently treated with cycloheximide (CHX, 50 μg/mL) in the presence or absence of bafilomycin A1 (BafA1, 50 nM), chloroquine (CQ, 10 μM), or 3-methyladenine (3-MA, 10 mM) for 6 h, followed by Western blot analysis with the indicated antibodies (bottom). *$P < 0.05$, **$P < 0.01$, ***$P < 0.001$, ****$P < 0.0001$; Unpaired Student's *t*-test. Data are means ± SEM of at least three independent experiments.

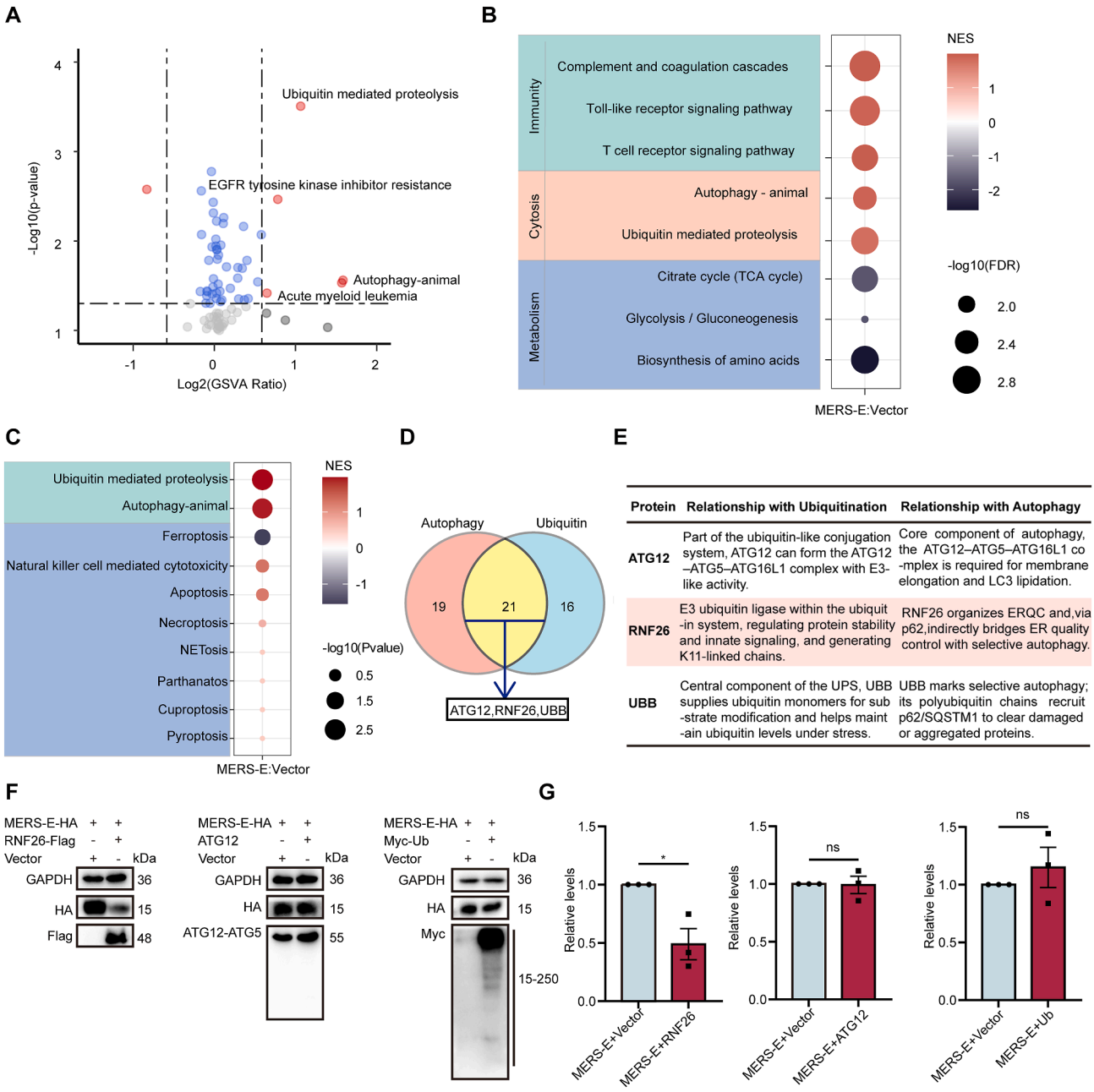

Protein	Relationship with Ubiquitination	Relationship with Autophagy
ATG12	Part of the ubiquitin-like conjugation system, ATG12 can form the ATG12 –ATG5–ATG16L1 complex with E3-like activity.	Core component of autophagy, the ATG12–ATG5–ATG16L1 co -mplex is required for membrane elongation and LC3 lipidation.
RNF26	E3 ubiquitin ligase within the ubiquit -in system, regulating protein stability and innate signaling, and generating K11-linked chains.	RNF26 organizes ERQC and,via p62,indirectly bridges ER quality control with selective autophagy.
UBB	Central component of the UPS, UBB supplies ubiquitin monomers for sub -strate modification and helps maint -ain ubiquitin levels under stress.	UBB marks selective autophagy; its polyubiquitin chains recruit p62/SQSTM1 to clear damaged or aggregated proteins.

Fig. 2. Proteomic profiling reveals coordinated activation of autophagy and ubiquitin–proteasome pathways by MERS-E. **A** Volcano plot of pathway scores for MERS-E versus control proteomes based on GSVA algorithm and KEGG database. Significantly altered pathways are labeled as red dots. **B-C** Bubble plot of the enrichment results of representative pathways (**B**) and typical cytosis pathways (**C**) by GSEA algorithm between the proteome of MERS-E and control groups based on KEGG database. **D** Venn diagram of proteins associated with autophagy and ubiquitin process among differentially expressed proteins ($P < 0.05$, $|FC| \geq 1.5$) between MERS-E and control proteomes. **E** Summary table showing the representative functions of three dual-pathway regulators (ATG12, RNF26, and UBB) identified from the intersection of autophagy- and ubiquitin-related differentially expressed proteins. Their relationships with ubiquitination (left) and autophagy (right) are summarized based on published literature. **F** HEK293T cells were co-transfected with the MERS-E-HA expression plasmid and either the RNF26-Flag, ATG12, or Myc-Ub expression plasmid, respectively, using an empty vector as a control. **G** Quantification of MERS-E protein expression by densitometric analysis using ImageJ ($N = 3$). $^{*}P < 0.05$, $^{**}P < 0.01$, $^{***}P < 0.001$, $^{****}P < 0.0001$; Unpaired Student's t-test. Data are means ± SEM of at least three independent experiments.

unique opportunity to link ubiquitin tagging with autophagic degradation (Jongsma et al., 2016; Cremer et al., 2021, 2023) (Fig. 2E). To experimentally validate this prioritization, we next performed comparative assays to examine the effects of these candidates on MERS-E protein abundance. Compared with vector control, co-expression of ATG12 had minimal effect on MERS-E levels. Because UBB encodes ubiquitin, a Myc-Ub expression construct was used to assess the effect of ubiquitin overexpression, which resulted in only a modest increase in MERS-E abundance. In contrast, co-expression of RNF26-Flag with MERS-E-HA markedly reduced MERS-E protein levels (Fig. 2F, G). Taken together, these results indicate that RNF26 exhibits the most prominent and consistent regulatory effect on MERS-E protein abundance among the tested candidates. Based on both its functional relevance and experimental validation, RNF26 was therefore selected for subsequent mechanistic investigation to further explore its role in the regulation of MERS-E.

RNF26 acts as a host restriction factor that mediates autophagic degradation of MERS-E

To determine whether RNF26 modulates the stability of the MERS-CoV envelope protein (MERS-E), we co-expressed MERS-E-HA with RNF26-Flag. In parallel, MERS-E was co-transfected with EGFP or empty vector as negative controls. Immunoblot analysis revealed that RNF26 overexpression markedly reduced MERS-E protein abundance compared with both control groups (Fig. 3A). Confocal microscopy confirmed this observation, showing a substantial decrease in MERS-E fluorescence intensity in cells co-expressing RNF26 (Fig. 3B). The same trend was consistently observed in both HEK293T and H292 cells, indicating that the regulatory effect of RNF26 is not cell-type specific. To further define this regulation, we titrated RNF26 expression while maintaining constant MERS-E plasmid levels. Increasing RNF26 expression resulted in a stepwise and proportional decline in MERS-E protein levels, establishing a clear dose-dependent suppression (Fig. 3C). Conversely, silencing endogenous RNF26 restored MERS-E accumulation (Fig. 3D), supporting a specific role for RNF26 in limiting MERS-E abundance. In contrast, increasing MERS-E expression did not alter RNF26 protein levels, and RNF26 expression likewise remained unchanged during MERS-CoV infection (Supplementary Fig. S3A–B), indicating that this regulatory relationship is not accompanied by detectable changes in RNF26 abundance. Importantly, the effect of RNF26 was preserved in a MERS-CoV infection model, where RNF26 overexpression reduced MERS-E levels in infected cells (Fig. 3E). RNF26 overexpression was also associated with lower viral titers, although this trend did not reach statistical significance (Fig. 3F). Moreover, RNF26 similarly reduced the abundance of SARS-CoV-2 E and HCoV-OC43 E proteins (Supplementary Fig. S3C–D), suggesting that its regulatory effect on coronavirus E proteins may extend beyond MERS-CoV. To further delineate the degradation mechanism, we employed pharmacological inhibitors targeting distinct steps of protein clearance under RNF26-MERS-E co-expression conditions. Blocking autophagy initiation with 3-MA markedly restored MERS-E protein levels, whereas inhibition of lysosomal acidification by CQ or BafA1 and proteasomal blockade by MG132 showed little effect (Fig. 3G). Mechanistically, co-expression of RNF26 and MERS-E further enhanced autophagic activity, as evidenced by elevated LC3-II levels and accelerated degradation of p62 compared with MERS-E alone (Fig. 3H). In parallel, lysosomal blockade with BafA1 under RNF26 overexpression conditions led to further accumulation of LC3-II and partially restored MERS-E-HA levels (Fig. 3I), supporting the involvement of an autophagy-lysosome pathway in RNF26-mediated MERS-E turnover. Consistent with these biochemical results, the tandem mRFP-EGFP-LC3 reporter assay revealed that MERS-E expression alone increased the formation of red-only puncta (autolysosomes), reflecting enhanced autophagic flux; this effect was further amplified in the presence of RNF26 (Fig. 3J). In addition, an LC3-based dual-luciferase reporter assay showed that MERS-E significantly increased reporter activity relative to the vector control, and co-expression of RNF26 with MERS-E further enhanced this signal (Fig. 3K), providing additional support that RNF26 augments autophagy-related responses in the presence of MERS-E. Together, these results support the notion that RNF26 augments autophagy-related responses and promotes at least partly lysosome-dependent degradation of MERS-E.

The E3 ligase activity of RNF26 is required for MERS-E degradation and maintenance of ER homeostasis

To define the structural basis of RNF26-mediated MERS-E degradation, we focused on its RING domain—a canonical zinc-finger motif of RING-type E3 ubiquitin ligases, which typically coordinate Zn^{2+} via conserved cysteine and histidine residues to catalyze ubiquitin transfer (Cai et al., 2022). Based on this motif, we generated four site-specific mutants (C395S, C399S, C401S, and Y432A) and a truncation lacking the entire RING domain (ΔRING). Each mutant was co-expressed with MERS-E in HEK293T cells, and their effects on MERS-E protein abundance were examined by immunoblotting. Among these variants, RNF26-C399S and RNF26-ΔRING lost the ability to promote E protein degradation, whereas the other point mutants retained partial activity (Fig. 4A). These results indicate that the catalytic integrity of the RING domain, particularly residues surrounding Cys399, is essential for RNF26-dependent E protein clearance. We next evaluated whether disruption of RNF26's catalytic function alters the cellular response to MERS-E protein stress. Co-expression of wild-type RNF26 ($RNF26^{WT}$) markedly improved cell viability, as quantified by flow cytometric analysis of PI-positive cells, confirming its protective effect against MERS-E–induced cytotoxicity. In contrast, cells expressing RNF26-C399S or RNF26-ΔRING exhibited persistently high proportions of PI-positive populations and reduced viability, consistent with the accumulation of undegraded E protein (Fig. 4B–C, Supplementary Fig. S4A). These data demonstrate that RNF26 mitigates MERS-E protein–induced cell death through a degradation-dependent mechanism. Given that E protein accumulation imposes membrane stress on the endoplasmic reticulum (ER), we first examined the spatial relationship between RNF26 and MERS-E. Confocal microscopy revealed that RNF26 and MERS-E-mCherry exhibited colocalization along the ER network, indicating that RNF26 is recruited to E-induced stress sites (Fig. 4D, Supplementary Fig. S4B). We next asked whether the catalytic activity of RNF26 influences ER stress signaling. Using an ER stress response element (ERSE)–driven dual-fluorescence reporter, we quantified unfolded protein response (UPR) activation. MERS-E expression alone increased ERSE activity, reflecting enhanced ER stress. Co-expression with RNF26-WT further augmented ERSE reporter output, suggesting that RNF26 amplifies the adaptive response to mitigate local proteotoxicity. In contrast, this induction was markedly blunted when MERS-E was co-expressed with RNF26-C399S or RNF26-ΔRING mutants, indicating that the RING-dependent catalytic function is required for RNF26-mediated coordination of ER stress adaptation (Fig. 4E, Supplementary Fig. S4C). To further define the UPR branch involved, we examined the PERK pathway under RNF26 overexpression conditions in the presence of MERS-E. RNF26 overexpression enhanced PERK pathway activation, as indicated by increased levels of phospho-PERK, phospho-eIF2α, and ATF4 at the protein level (Fig. 4F). At the transcript level, co-expression of RNF26 with MERS-E significantly increased the mRNA levels of CHOP, GADD34, and BIP, whereas ATF4, PERK, and EIF2α mRNA levels were not significantly altered (Supplementary Fig. S4D). This pattern is consistent with a phosphorylation-dependent mode of PERK signaling, and the increase in ATF4 protein in the absence of a corresponding change in ATF4 mRNA further supports translational regulation downstream of eIF2α phosphorylation. Together with the ERSE reporter results and the requirement for the RNF26 RING domain, these findings indicate that RNF26 enhances MERS-E-induced UPR signaling, particularly along the PERK-eIF2α-ATF4 axis. Together, these findings reveal that RNF26 requires an intact RING domain to catalyze E protein degradation, preserve ER homeostasis, and prevent stress-induced cytotoxicity. Mechanistically, the failure of catalytic mutants to remove MERS-E protein results in sustained ER burden and impaired UPR tuning, supporting a model in which RNF26 couples ubiquitin-mediated degradation to stress adaptation at the ER interface.

DISCUSSION

This study reveals a dual role of the MERS-E in host cells. On one hand, E expression reduces cell viability and robustly induces autophagy. On the other, its degradation depends on the host ER-anchored E3 ubiquitin ligase RNF26 through an autophagy–lysosome pathway. We further show that MERS-E expression enhances ER stress and activates ERSE-driven transcription, whereas impairment of RNF26 function leads to E accumulation and amplification of the stress response, forming a self-reinforcing ER-stress–autophagy feedback loop. Together,

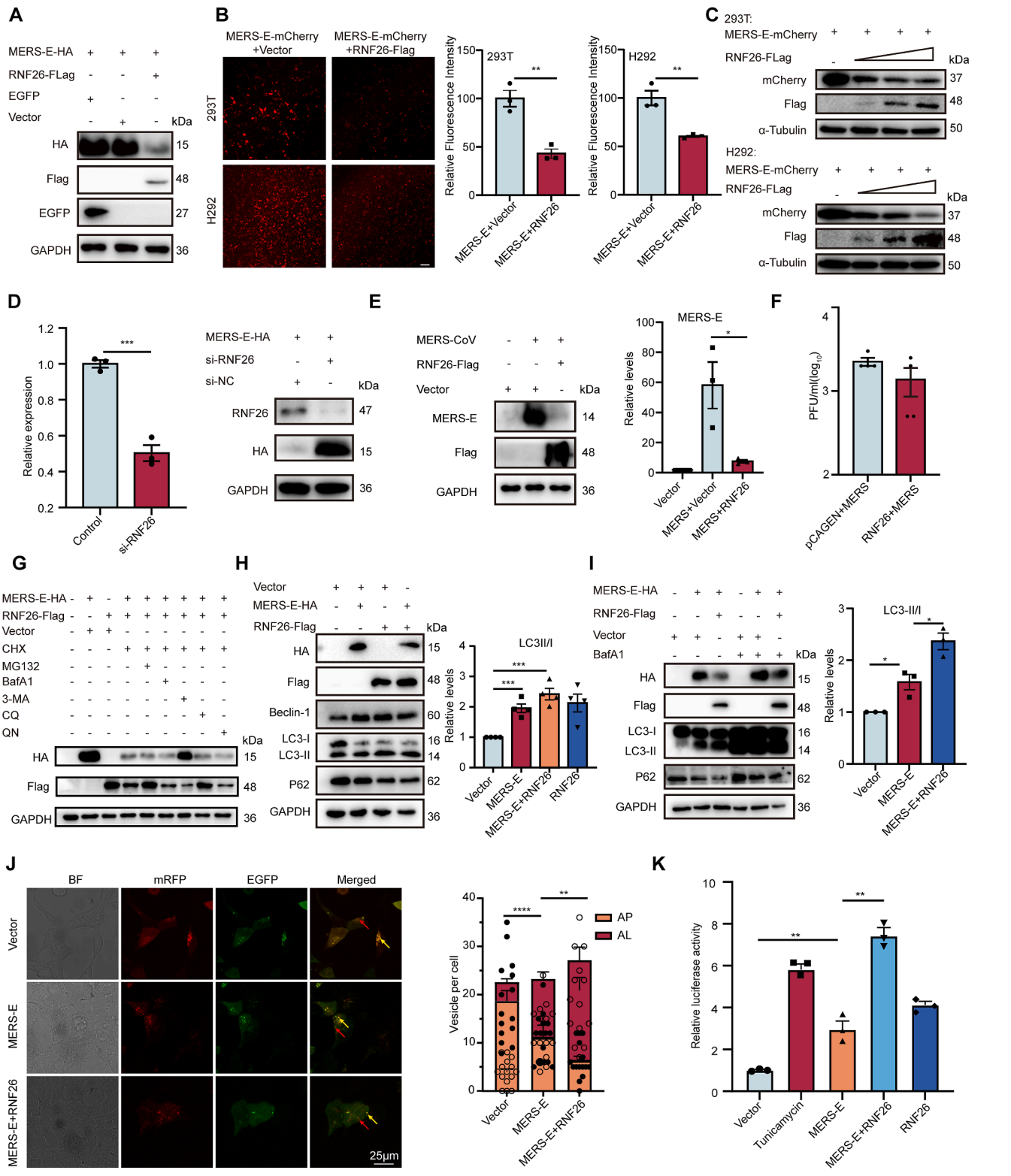

(caption on next page)

Fig. 3. RNF26 acts as a host restriction factor that mediates autophagic degradation of MERS-E. **A** HEK293T cells were transfected with the indicated plasmids (MERS-E-HA, RNF26-Flag, EGFP or empty vector) for 24 h and analyzed by Western blot with indicated antibodies. **B** HEK293T and H292 cells were co-transfected with MERS-E-mCherry and either empty vector or RNF26-Flag plasmid. Fluorescence microscopy was used to visualize MERS-E-mCherry expression (left). Quantification of relative fluorescence intensity was performed using ImageJ from three independent experiments (right). Scale bars, 100 μm. **C** HEK293T and H292 cells were co-transfected with a constant amount of MERS-E-mCherry plasmid and increasing amounts of RNF26-Flag plasmid for 24 h and analyzed by Western blotting with the indicated antibodies. **D** The knockdown efficiency of si-RNF26 as determined by qPCR (left). HEK293T cells were co-transfected with MERS-E-HA plasmid and siRNA targeting RNF26 (si-RNF26, sequence GTGGGCAAGACCCTTGGAA) or control siRNA (si-NC) for 24 h, followed by Western blot analysis. **E** HEK293T-hDPP4 cells (HEK293T cells stably expressing human DPP4, the receptor for MERS-CoV) were transfected with RNF26-Flag or empty vector and then infected with MERS-CoV as indicated (left). Quantification of MERS-E expression (right) by densitometric analysis using ImageJ ($N = 3$). **F** HEK293T-hDPP4 cells were transfected with RNF26-Flag or empty vector (pCAGEN) and then infected with MERS-CoV. Viral replication was assessed by plaque assay, and the results are presented as PFU/mL ($\log_{10}$; $N = 4$). **G** HEK293T cells were co-transfected with MERS-E-HA and RNF26-Flag plasmids or empty vector for 24 h and subsequently treated with CHX (50 μg/mL) in the presence or absence of MG132 (5 μM), BafA1 (50 nM), CQ (10 μM), 3-MA (10 mM), or quinacrine (QN, 10 μM) for 6 h, followed by Western blot analysis with the indicated antibodies. **H** HEK293T cells were co-transfected with MERS-E-HA and RNF26-Flag plasmids or empty vector for 24 h and analyzed by Western blot with the indicated antibodies (left). Quantification of LC3-II/I expression (right) by densitometric analysis using ImageJ ($N = 4$). **I** HEK293T cells were transfected with MERS-E-HA, RNF26-Flag, or empty vector as indicated. After 24 h, cells were treated with or without BafA1 (50 nM) for 6 h (left). Quantification of LC3-II/I expression (right) by densitometric analysis using ImageJ ($N = 3$). **J** mRFP-EGFP-LC3 fluorescence assay showing autophagic flux in HEK293T cells transfected with vector, MERS-E, or co-transfected with MERS-E and RNF26. Cells were imaged 24 h after transfection under a confocal microscope (left). Yellow puncta (merged mRFP and EGFP signals, indicated by yellow arrows) represent autophagosomes (AP), and red-only puncta (indicated by red arrows) represent autolysosomes (AL). Scale bars, 25 μm. Quantification of AP and AL vesicles numbers per cell (right). Quantification was performed from 15 independent cells ($N = 15$). **K** HEK293T cells were transfected with vector, MERS-E-HA, MERS-E-HA + RNF26-Flag, or RNF26-Flag as indicated, together with an LC3-based dual-luciferase reporter system. For the tunicamycin group, vector-transfected cells were treated with tunicamycin (1 μg/mL) for 6 h at 24 h post-transfection. Quantification was performed from 3 independent experiments ($N = 3$). $^{*}P < 0.05$, $^{**}P < 0.01$, $^{***}P < 0.001$, $^{****}P < 0.0001$; Unpaired Student's *t*-test. Data are means ± SEM of at least three independent experiments.

these findings delineate a "membrane homeostatic conflict" in which the host attempts to eliminate abnormal membrane proteins through autophagy, while viral E protein disrupts ER quality control (ERQC) and thereby undermines this protective mechanism.

Proteomic enrichment analysis revealed that pathways related to autophagy and ubiquitination were markedly upregulated in MERS-E-expressing cells, suggesting a broad rewiring of the protein degradation network. Molecular and morphological evidence indicated increased LC3 lipidation, reduced p62 levels, and formation of autophagosomes, supporting the notion that cells engage the autophagy pathway to mitigate viral protein load. Pharmacological inhibition of autophagy (by 3-MA) caused marked restoration of E protein levels, implying that E serves as a selective substrate of the autophagy-lysosome system. In viral infection contexts, autophagy exhibits a well-recognized "dual character". It can function as a host defense mechanism that selectively removes viral components or damaged organelles, thereby limiting replication and cytotoxicity (Zhai et al., 2023). Conversely, many viruses co-opt the autophagy machinery to promote their own propagation by blocking autophagosome–lysosome fusion or exploiting autophagic membranes for virion assembly (Wang and Ou, 2015; Hou et al., 2023; Hsu et al., 2025; Wang et al., 2025). For example, the SARS-CoV-2 ORF3a protein impairs the HOPS complex and arrests autophagic flux, preventing its own degradation while facilitating viral egress (Zhang et al., 2021). In contrast, MERS-E triggered a functionally competent autophagy flux in which the protein itself was cleared as a degradation substrate, representing a defensive and self-protective host response. Such "defensive autophagy" is likely beneficial during early infection, yet under persistent stress or impaired clearance it may become maladaptive, predisposing cells to the sustained ER stress observed here.

We identify RNF26 as a key host restriction factor that mediates MERS-E clearance. RNF26 resides in the ER membrane and serves as a pivotal E3 ligase that bridges ubiquitination and autophagic degradation pathways. Our data demonstrate that RNF26 promotes MERS-E autophagic degradation in a RING-dependent manner; loss of catalytic integrity through C399S or ΔRING mutations abolishes this clearance and exacerbates E-induced cytotoxicity. Previous studies have shown that RNF26 forms a complex with the E2 enzyme UBE2J1, generates active ubiquitin chains in the perinuclear ER, and recruits UBD-containing adaptors such as p62/SQSTM1, TOLLIP, and TAX1BP1, thereby coupling ER-associated quality control with endolysosomal degradation (Jongsma et al., 2016; Cremer et al., 2021, 2023). Integrating these observations, we propose that RNF26 performs dual and potentially complementary functions under viral membrane stress. First, as an E3 ligase, it catalyzes K63-linked or functionally equivalent ubiquitination of MERS-E, allowing selective recognition by autophagy receptors and subsequent routing to lysosomal degradation. Second, RNF26 may act as a spatial scaffold that coordinates local autophagosome–lysosome dynamics, thereby enhancing the efficiency of membrane protein turnover. These mechanisms are not mutually exclusive and likely operate in concert to maintain proteostatic equilibrium during viral infection. Consistent with this model, ERSE reporter assays revealed that MERS-E expression activates ER stress, and this response becomes markedly intensified when RNF26 function is disrupted or autophagy is blocked. Together, these findings suggest that RNF26 acts as a molecular buffer that links ubiquitin-mediated degradation to ER stress adaptation. When this coordination fails, E protein accumulates within the ER, leading to sustained unfolded protein response activation and progressive loss of degradative capacity. Over time, this imbalance amplifies cellular stress and compromises survival, establishing a feed-forward cycle in which impaired clearance and ER dysfunction reinforce each other.

Based on these results, we propose an integrative model describing the dynamic interplay between MERS-E and the host protein quality control network. Excessive MERS-E accumulation is sensed as proteotoxic stress, activating RNF26-mediated ubiquitination and selective autophagic clearance to restore membrane homeostasis. Under conditions of RNF26 loss or system overload, MERS-E escapes degradation, amplifies UPR signaling, and disrupts ERQC efficiency, ultimately leading to cell dysfunction and inflammation (Fig. 5). This model underscores a fundamental principle: the host cell is not merely a passive victim of viral membrane stress but actively mobilizes the ERQC-autophagy network as a protective response. Yet once this adaptive circuit is overwhelmed, defensive autophagy transforms into pathogenic feedback that amplifies ER stress and cell injury. In addition, our data suggest that RNF26 may modulate MERS-E–induced ER stress, with a predominant effect on the PERK branch of the UPR. Rather than simply reflecting a passive consequence of protein accumulation, this enhancement of PERK signaling may indicate that RNF26-associated ERQC processes contribute to shaping the cellular stress response. In this context, RNF26 may influence the recognition or processing of membrane-associated proteotoxic stress, thereby facilitating PERK-dependent signaling as part of an adaptive response. However, under sustained or excessive stress conditions, such effects may become maladaptive, consistent with the transition from protective to pathogenic UPR signaling. By linking RNF26 directly to the selective clearance of a viral membrane protein, our study extends the biological repertoire of

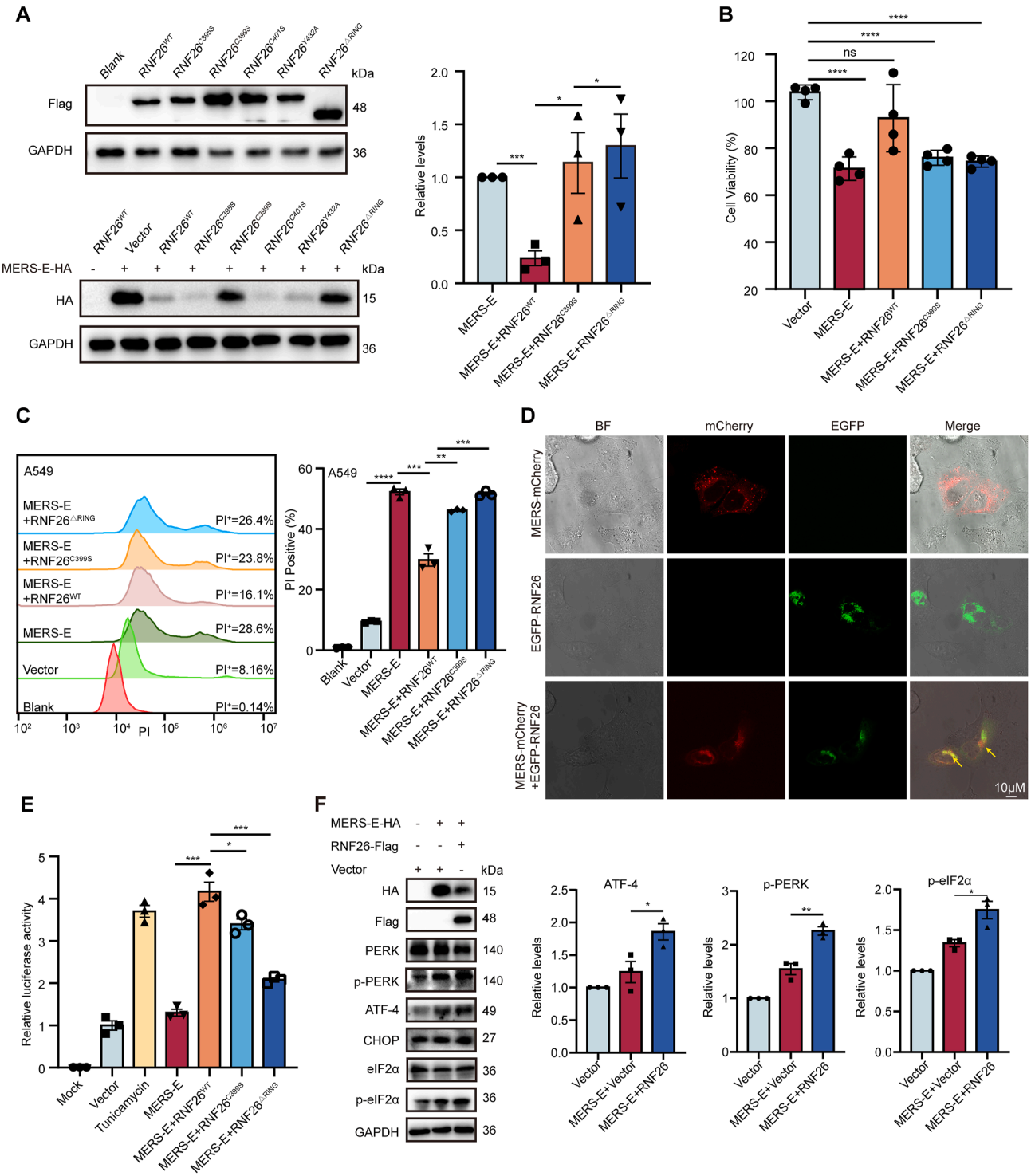

Fig. 4. The E3 ligase activity of RNF26 is required for MERS-E degradation and maintenance of ER homeostasis. **A** HEK293T cells were transfected with wild-type RNF26 or the indicated RNF26 mutants alone (top) or co-transfected with MERS-E-HA (bottom) for 24 h and analyzed by Western blotting with the indicated antibodies. Quantification of MERS-E-HA expression (right) by densitometric analysis using ImageJ ($N = 3$). **B** Cell viability of HEK293T cells transfected with the indicated plasmids for 24 h. **C** Flow cytometry histograms (left) and quantification of PI-positive cells (right) in H292 and A549 cells transfected with the indicated plasmids for 24 h. **D** HEK293T cells were transfected with MERS-E-mCherry, EGFP-RNF26, or both plasmids for 24 h. Confocal fluorescence microscopy was used to visualize the subcellular localization and co-localization of MERS-E-mCherry and EGFP-RNF26, with yellow signals in the merged images indicating co-localization (yellow arrows). Scale bar, 10 μm. **E** Dual-luciferase assay assessing the impact of co-transfected expression plasmids on ERSE promoter activity in HEK293T cells. Tunicamycin (1 μg/mL) treatment served as a positive control for ER stress induction. Quantification was performed from 3 independent experiments. **F** HEK293T cells were co-transfected with MERS-E-HA and RNF26-Flag or empty vector as indicated, and the protein levels of UPR-related markers were analyzed by Western blotting (left). Quantification of UPR-related protein expression (right) by densitometric analysis using ImageJ ($N = 3$). $^{*}P < 0.05$, $^{**}P < 0.01$, $^{***}P < 0.001$, $^{****}P < 0.0001$; Unpaired Student's *t*-test. Data are means ± SEM of at least three independent experiments.

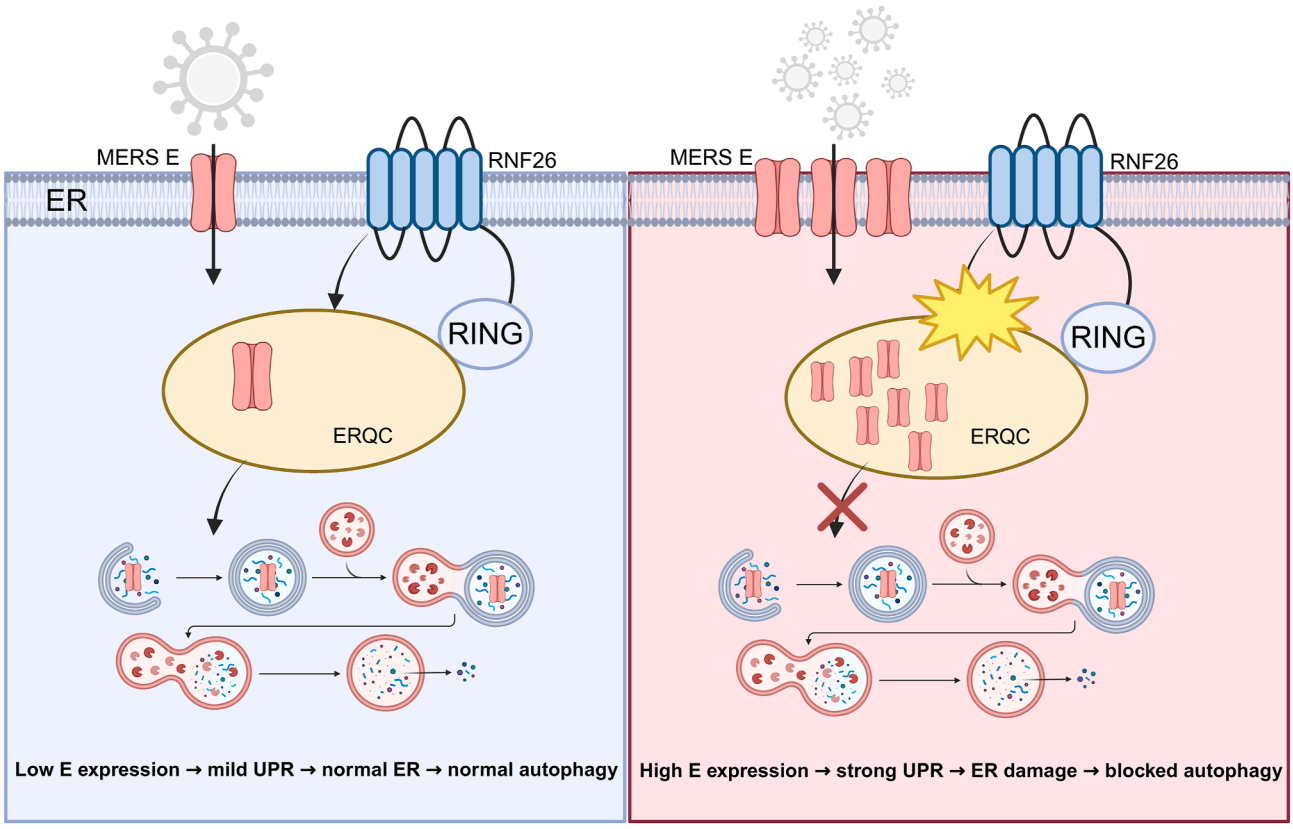

Fig. 5. Schematic model illustrating how RNF26 modulates ER homeostasis and autophagy under different MERS-E expression levels. At low viral load (left panel), MERS-E interacts with RNF26 at the endoplasmic reticulum (ER) and is recruited to the ER quality control compartment (ERQC), leading to mild unfolded protein response (UPR) activation and normal autophagy. At high viral load (right panel), excessive MERS-E accumulation causes severe ER stress and UPR activation, resulting in ER damage, disruption of ERQC, and autophagy blockade.

this E3 ligase beyond canonical ERQC to antiviral defense. Although RNF26 required its RING domain, we did not obtain reproducible evidence for stable direct interaction or direct ubiquitination of MERS-E under the conditions tested. Thus, RNF26 may regulate MERS-E through an indirect ERQC-associated mechanism. Notably, RNF26 protein levels remained unchanged upon MERS-E expression or during viral infection, indicating that RNF26 is not regulated by MERS-E. This observation supports a unidirectional regulatory model in which RNF26 acts upstream to control MERS-E abundance, rather than being induced as part of a feedback response. The proposed ERQC-autophagy feedback model provides a conceptual framework for understanding how host protein-quality-control networks counteract viroporin-induced stress and suggests that pharmacological enhancement of selective autophagy or ERQC capacity could represent a promising host-directed antiviral strategy.

CONCLUSIONS

In conclusion, this study demonstrates that the MERS-CoV envelope protein disrupts host proteostasis by inducing ER stress and autophagy. We identify the ER-anchored E3 ubiquitin ligase RNF26 as a key host factor that promotes MERS-E clearance through an autophagy-lysosome-dependent pathway, thereby limiting E protein accumulation and alleviating E-induced cytotoxic stress. This process requires the catalytic integrity of the RNF26 RING domain and is associated with the maintenance of ER homeostasis. Together, our findings reveal an RNF26–ERQC–autophagy axis that functions as a host protective mechanism against coronavirus E protein-induced membrane stress, providing new insight into viral membrane protein quality control and potential host-directed antiviral strategies.

MATERIALS AND METHODS

Plasmids and mutagenesis

Wild-type MERS-CoV-E (GenBank: ALK80316.1) and RNF26 (GenBank: NP_114404.1) sequences were synthesized by BGI (Beijing Genomics Institute, China) and cloned into the eukaryotic expression vector pcDNA3.1. Point mutations were generated using site-directed mutagenesis and confirmed by sequencing.

Cell culture

HEK293T, H292, A549 and 16HBE cells were purchased from National Collection of Authenticated Cell Cultures, China. HEK293T and H292 cells were cultured in 90% DMEM basal medium (Gibco, Grand Island, NY, USA, C11965500BT), and A549 cells were cultured in 90% RPMI-1640 basal medium (Gibco, USA, C11875500CP), supplemented with 10% fetal bovine serum (FBS; Gibco, USA, A5670701). 16HBE epithelial cells were cultured in Keratinocyte Medium (ScienCell Research Laboratories, Carlsbad, CA, USA, 2101) according to the manufacturer's instructions, without serum supplementation.

Cell viability assay

Cells were seeded at a density of 8000 cells per well in 96-well plates and transfected the next day with the indicated plasmids using Lipofectamine 3000 reagent (Thermo Fisher Scientific, Waltham, MA, USA, L3000075) according to the manufacturer's instructions for 24 h. Cell viability was assessed using a CCK-8 kit (Yeasen Biotechnology, Shanghai, China, 40203ES60) following the manufacturer's

instructions. Absorbance was measured at 450 nm using a microplate reader (Thermo Fisher Scientific, Waltham, MA, USA).

Western blot assay and antibodies

Proteins were resolved in 12% SDS-PAGE, transferred to PVDF membranes (GE Healthcare Life Sciences, Little Chalfont, Buckinghamshire, UK), and incubated with primary antibodies against HA-Tag (C29F4) (3724, Cell Signaling Technology, Danvers, MA, USA), GAPDH (30201ES20, Yeasen, China), mCherry (ab125096, Abcam, Cambridge, UK), Flag (14793, CST, USA), LC3 (3868, CST, USA), Beclin-1 (3495, CST, USA), P62 (5114, CST, USA), RIPK1 (3493S, CST, USA), RIPK3 (13526, CST, USA), p-RIPK3 (93654S, CST, USA), MLKL (14993S, CST, USA), p-MLKL (91689S, CST, USA), Caspase-3 (14220T, CST, USA), Caspase-7 (12827T, CST, USA), GSDME (19453, CST, USA), PERK (3192, CST, USA), p-PERK (3179, CST, USA), eIF2α (9722, CST, USA), p-eIF2α (3398, CST, USA), ATF-4 (11815, CST, USA), CHOP (2895, CST, USA), and GSDMC (61921, CST, USA). Secondary antibodies were peroxidase-conjugated goat anti-rabbit IgG (H + L) (33101ES60, Yeasen, China) and peroxidase AffiniPure goat anti-mouse IgG (H + L) (33201ES60, Yeasen, China).

Flow cytometry of cell death

After treatment, cells were detached, collected by centrifugation, and resuspended in 1 × binding buffer containing 2 μg/mL propidium iodide (PI), followed by incubation at room temperature for 15 min in the dark. Subsequently, 400 μL of 1 × binding buffer was added, and the cells were kept on ice. Samples were analyzed by flow cytometry using a BD FACSCalibur™ system (BD Biosciences, San Jose, CA, USA), and the percentages of differently labeled cells were calculated using FlowJo software (version 7.6).

qRT-PCR analysis

Total RNA was extracted from cells and tissues using the Trizol reagent (Invitrogen, USA) and the total nucleic acid extraction kit (Ambion, Austin, TX, USA), respectively, as per the manufacturers' instructions. Quantitative PCR was performed using SYBR Green Master Mix (11184ES03, Yeasen, China) to determine the mean ΔCt values and the standard error of the mean (SEM). Primer sequences used for qPCR are listed in Table S1.

Confocal fluorescence imaging

Imaging was performed using a Leica TCS-SP8 STED inverted laser confocal microscope with 40 × and 100 × objectives for high-resolution acquisition. Appropriate laser channels were selected according to the wavelengths of the fluorescent labels, and laser intensity, gain, pinhole, and scanning speed were adjusted to optimize signal quality. Fluorescent signal acquisition and image capture were carried out using the LAS X software (Leica Microsystems, Wetzlar, Germany).

Proteome sample preparation

H292 cells were washed with cold PBS and lysed in SDT buffer (4% SDS, 100 mM Tris-HCl, 100 mM DTT, pH 7.6). The lysates were heated at 95 °C for 10 min and centrifuged at 15,000×*g* for 15 min. Protein concentrations were determined using a tryptophan fluorescence assay. A total of 100 μg protein from each sample was alkylated with 350 mM iodoacetamide (25 °C, 45 min, in the dark). Proteins were purified using the SP3 method and digested overnight with trypsin (enzyme-to-protein ratio 1:100) at 37 °C. Peptides were acidified with 10% trifluoroacetic acid, desalted, and dried for LC-MS/MS analysis.

LC-MS/MS analysis

The DIA analysis was performed on a hybrid TIMS quadrupole TOF mass spectrometer (Bruker timsTOF Pro) platform connected to an online nanoflow U3000 HPLC system (Thermo Fisher Scientific, USA).

Database searching and data analysis

Raw data were processed using Spectronaut software against the Uniprot human proteome database, with precursor FDR at 1%.

Function enrichment analysis

Gene function enrichment analysis was performed with the R Bioconductor package 'clusterProfiler' (R package version 3.14.3) based on Gene Ontology (GO) database or Kyoto Encyclopedia of Genes and Genomes (KEGG) database. Enrichment scores were determined using Fisher's exact test.

GSEA/GSVA

Gene set enrichment analysis (GSEA) and gene set variation analysis (GSVA) were performed by "clusterProfiler" (R package v4.10.1) and GSVA (R package 1.50.5) packages respectively based on human KEGG datasets downloaded from the Molecular Signature Database MSigDB (https://www.kegg.jp).

Venn diagram analysis

We searched PubMed to annotate the functions of 111 proteins that were significantly altered in the proteomic analysis following MERS-E overexpression. Each protein was evaluated based on existing literature to determine whether it was involved in the autophagy pathway, the ubiquitin–proteasome pathway, or both.

TEM

HEK293T cells were transfected with either the MERS-E expression plasmid or the empty vector for 24 h. Cell pellets (approximately 1 mm^3) were collected and fixed overnight at 4 °C with 2.5% glutaraldehyde. On the second day, the fixatives were removed, and the cells were washed by the PBS, and then fixed by 1% osmic acid at room temperature. After 1.5 h, the cells were dehydrated with 30%, 50%, 70%, 80%, 95%, and 100% ethanol for 15 min. Next, the supernatants were replaced with 100% acetone twice. Cells were infiltrated with Epon812/acetone (1:1) mixture for 2–3 h, then replaced with pure Epon812 overnight. At last, the samples were polymerized at 60 °C for 48 h. Ultrathin sections (70 nm) were obtained by using diamond knife and collected on slot grids. The grids were post-stained with 2% uranyl acetate and lead citrate. Sections were analyzed with a Tecnai G2 Spirit Twin (FEI) plus transmission electron microscope equipped with a camera (Gatan, Inc, Pleasanton, CA, USA). The samples were fixed for >7 days at 4 °C using 2.5% glutaraldehyde in 0.1 M phosphate buffer (PB) (pH 7.2), and then washed with 0.1 M PB (pH 7.2) three times for 7 min. Afterward, samples were postfixed with 1% OsO_4 for 2h at 4 °C, and then washed with ddH_2O three times for 7 min, followed by serial ethanol dehydration and acetone transition for 5 min, embedding in Epon 812 resin, polymerization at 60 °C for 48 h. Serial sections of 60 nm thickness were made using a Leica EM UC7 ultramicrotome. Ultrathin sections were then loaded onto 100 mesh Cu grids and double stained with 2% uranyl acetate and lead citrate before observations employing a JEM-1400 Plus transmission electron microscope at 80 kV.

Dual-luciferase reporter assay

Cells were seeded at a density of 8×10^3 cells per well in 96-well plates and transfected with the indicated plasmids the next day. After 24 h of transfection, luciferase activities were measured using the Dual-Luciferase Reporter Assay Kit (Beyotime Biotechnology, Shanghai, China, RG027) according to the manufacturer's instructions. For each well, 50–100 μL of reporter lysis buffer was added, and the cells were lysed on a shaker at 37 °C for 20–30 min. The lysates were then transferred to a white opaque 96-well plate, followed by the addition of 50 μL of firefly luciferase detection reagent to each well. The mixture was gently mixed, and luminescence was immediately measured using a multifunctional microplate reader equipped with a chemiluminescence detection module. Subsequently, 50 μL of Renilla luciferase detection reagent was added to each well, and the luminescence was measured again. The relative luciferase activity (RLA) was calculated as the ratio of firefly to Renilla luciferase relative light units (RLU) to compare the relative activation levels of ERSE among different groups.

Virus

MERS-CoV EMC/2012 (GenBank accession no.: JX869059.2) was a kind gift from R. Fouchier (Erasmus Medical Center, Rotterdam, The Netherlands). MERS-CoV infection experiments were performed in accordance with the approved standard operating procedures of our Block T Physical Containment Level 3 (BTPC3) Laboratory, at the Department of Microbiology, The University of Hong Kong.

MERS-CoV infection

HEK293T-hDPP4 cells were seeded in 6-well plates at a density of 5×10^5 cells per well and cultured overnight to reach 70%–80% confluence. Cells were then transfected with 2 μg of either pCAGEN-RNF26 or empty pCAGEN vector per well using Lipofectamine 3000 (Thermo Fisher Scientific). At 24 h post-transfection, HEK293T-hDPP4 cells were infected with MERS-CoV at a multiplicity of infection (MOI) of 1 for 2 h at 37 °C, washed twice with PBS, replenished with fresh medium, and further incubated for 24 h at 37 °C with 5% CO_2.

Viral supernatants were collected at 24 h post-infection and clarified by centrifugation at 1000×*g* for 10 min to remove cell debris. Infectious titres of MERS-CoV were determined via standard plaque assays as we previously described (Chu et al., 2021, 2022). Briefly, Vero E6 cells were seeded in 12-well plates 24 h prior to the experiment. The collected supernatant samples were subjected to 10-fold serial dilution and inoculated onto the Vero E6 cells for 2 h at 37 °C; the cells were then washed three times with PBS and overlaid with a 1:1 mixture of 2% agarose (in PBS) and 2 × DMEM supplemented with 2% FBS. Following incubation at 37 °C with 5% CO_2 for 72 h, the cells were fixed with 4% paraformaldehyde. Fixed plates were stained with 0.5% crystal violet (dissolved in 25% ethanol in distilled water) for 10 min to visualize plaques. Viral titers were calculated as plaque-forming units per milliliter (PFU/mL) based on the number of plaques counted in the appropriate dilution wells.

DATA AVAILABILITY

All data for this article are available on the Science Data Bank (https://doi.org/10.57760/sciencedb.38185). The mass spectrometry raw data have also been deposited in iProX under accession number PXD069711 and are currently accessible through the editor URL (https://www.iprox.cn/page/SSV024.html?url=1761014569179L2xd) with the password Luc2.

AUTHOR CONTRIBUTIONS

Ziyue Li: Investigation, Methodology, Formal analysis, Validation, Visualization, Writing-original draft. Yang Wang: Investigation and Methodology for viral infection experiments. Jingbo Qie: Investigation, Methodology, and Data curation for proteomics experiments. Shuangqu Li: Investigation, Methodology, Validation. Zhaobing Gao: Conceptualization, Project administration, Supervision, Funding acquisition, Writing-review & editing. Hin Chu: Conceptualization, Supervision, Resources, Writing-review & editing. Bingqing Xia: Conceptualization, Project administration, Supervision, Funding acquisition, Writing-review & editing. Bingqing Xia, Zhaobing Gao, and Ziyue Li: Writing-original draft. All authors analyzed and discussed the data, read and approved the final manuscript.

CONFLICT OF INTEREST

The authors declare no competing interests.

ACKNOWLEDGEMENTS

We are grateful to the National Natural Science Foundation of China (82341058, 92169202), the Scientific Instrument Developing Project of the Chinese Academy of Sciences (PTYQ2024YZ0008), Fund of Shanghai Science and Technology (20ZR1474200, 22QA1411000), Fund of Shanghai Sailing Program (23YF1433100), Fund of Youth Innovation Promotion Association (Grants 2023078), Youth Inno the Science and Technology Commission of Shanghai Municipality (23JC1404300), and the National Key R&D Program of China (2023YFC2307800). Hin Chu acknowledges support from the Prevention and Control of Emerging and Major Infectious Diseases–National Science and Technology Major Project (2026ZD01911200 and 2026ZD01911201); the Health and Medical Research Fund (COVID1903010-14, 23220522, CID-HKU1-5), Food and Health Bureau, The Government of the Hong Kong Special Administrative Region; the General Research Fund (17118621, 17119122), Collaborative Research Fund (C7103-22G), and Theme-Based Research Scheme (T11-709/21-N), Research Grants Council of the Hong Kong Special Administrative Region; the InnoHK initiative of the Innovation and Technology Commission of the Hong Kong Special Administrative Region Government; the National Key Research and Development Program of China (2021YFC0866100 and 2023YFC3041600); the General Programme of the Guangdong Provincial Natural Science Foundation, China (2023A1515012325, 2023A1515011891); and support from Dr. Gallant Ho under the Gallant Ho Outstanding Young Professorship.

APPENDIX A. SUPPLEMENTARY DATA

Supplementary data to this article can be found online at https://doi.org/10.1016/j.virs.2026.06.005.

REFERENCES

Bello-Perez, M., Hurtado-Tamayo, J., Requena-Platek, R., Canton, J., Sánchez-Cordón, P. J., Fernandez-Delgado, R., Enjuanes, L., Sola, I., 2022. Mers-cov orf4b is a virulence factor involved in the inflammatory pathology induced in the lungs of mice. PLoS Pathog. 18, e1010834.

Cai, C., Tang, Y.D., Zhai, J., Zheng, C., 2022. The ring finger protein family in health and disease. Signal Transduct. Targeted Ther. 7, 300.

Castro-Gonzalez, S., Chen, Y., Benjamin, J., Shi, Y., Serra-Moreno, R., 2021. Residues t (48) and a(49) in hiv-1 nl4-3 nef are responsible for the counteraction of autophagy initiation, which prevents the ubiquitin-dependent degradation of gag through autophagosomes. Retrovirology 18, 33.

Chu, H., Shuai, H., Hou, Y., Zhang, X., Wen, L., Huang, X., Hu, B., Yang, D., Wang, Y., Yoon, C., Wong, B.H., Li, C., Zhao, X., Poon, V.K., Cai, J.P., Wong, K.K., Yeung, M.L., Zhou, J., Au-Yeung, R.K., Yuan, S., Jin, D.Y., Kok, K.H., Perlman, S., Chan, J.F., Yuen, K.Y., 2021. Targeting highly pathogenic coronavirus-induced apoptosis reduces viral pathogenesis and disease severity. Sci. Adv. 7, eabf8577.

Chu, H., Hou, Y., Yang, D., Wen, L., Shuai, H., Yoon, C., Shi, J., Chai, Y., Yuen, T.T., Hu, B., Li, C., Zhao, X., Wang, Y., Huang, X., Lee, K.S., Luo, C., Cai, J.P., Poon, V.K., Chan, C.C., Zhang, A.J., Yuan, S., Sit, K.Y., Foo, D.C., Au, W.K., Wong, K.K., Zhou, J., Kok, K.H., Jin, D.Y., Chan, J.F., Yuen, K.Y., 2022. Coronaviruses exploit a host cysteine-aspartic protease for replication. Nature 609, 785–792.

Cremer, T., Jongsma, M.L.M., Trulsson, F., Vertegaal, A.C.O., Neefjes, J., Berlin, I., 2021. The er-embedded ube2j1/rnf26 ubiquitylation complex exerts spatiotemporal control over the endolysosomal pathway. Cell Rep. 34, 108659.

Cremer, T., Voortman, L.M., Bos, E., Jongsma, M.L., Ter Haar, L.R., Akkermans, J.J., Talavera Ormeño, C.M., Wijdeven, R.H., de Vries, J., Kim, R.Q., Janssen, G.M., van Veelen, P.A., Koning, R.I., Neefjes, J., Berlin, I., 2023. Rnf26 binds perinuclear vimentin filaments to integrate er and endolysosomal responses to proteotoxic stress. EMBO J. 42, e111252.

Echavarría-Consuegra, L., Cook, G.M., Busnadiego, I., Lefèvre, C., Keep, S., Brown, K., Doyle, N., Dowgier, G., Franaszek, K., Moore, N.A., Siddell, S.G., Bickerton, E., Hale, B.G., Firth, A.E., Brierley, I., Irigoyen, N., 2021. Manipulation of the unfolded protein response: a pharmacological strategy against coronavirus infection. PLoS Pathog. 17, e1009644.

Feng, Y., Pan, Z., Wang, Z., Lei, Z., Yang, S., Zhao, H., Wang, X., Yu, Y., Han, Q., Zhang, J., 2022. Mers-cov nsp1 regulates autophagic flux via mtor signalling and dysfunctional lysosomes. Emerg. Microb. Infect. 11, 2529–2543.

Gassen, N.C., Niemeyer, D., Muth, D., Corman, V.M., Martinelli, S., Gassen, A., Hafner, K., Papies, J., Mösbauer, K., Zellner, A., Zannas, A.S., Herrmann, A., Holsboer, F., Brack-Werner, R., Boshart, M., Müller-Myhsok, B., Drosten, C., Müller, M.A., Rein, T., 2019. Skp2 attenuates autophagy through beclin1-ubiquitination and its inhibition reduces mers-coronavirus infection. Nat. Commun. 10, 5770.

Han, S.W., Jung, B.K., Ryu, K.Y., 2021. Regulation of polyubiquitin genes to meet cellular ubiquitin requirement. BMB Rep. 54, 189–195.

Hou, P., Wang, X., Wang, H., Wang, T., Yu, Z., Xu, C., Zhao, Y., Wang, W., Zhao, Y., Chu, F., Chang, H., Zhu, H., Lu, J., Zhang, F., Liang, X., Li, X., Wang, S., Gao, Y., He, H., 2023. The orf7a protein of sars-cov-2 initiates autophagy and limits autophagosome-lysosome fusion via degradation of snap29 to promote virus replication. Autophagy 19, 551–569.

Hsu, C.Y., Huang, W.R., Chiang, I.H., Li, J.Y., Munir, M., Liu, H.J., 2025. Avian reovirus induces autophagy-mediated cargo of progeny viruses to extracellular vesicles and enhancement of virus release. Vet. Microbiol. 307, 110627.

Jongsma, M.L., Berlin, I., Wijdeven, R.H., Janssen, L., Janssen, G.M., Garstka, M.A., Janssen, H., Mensink, M., van Veelen, P.A., Spaapen, R.M., Neefjes, J., 2016. An er-associated pathway defines endosomal architecture for controlled cargo transport. Cell 166, 152–166.

Klein, S., Cortese, M., Winter, S.L., Wachsmuth-Melm, M., Neufeldt, C.J., Cerikan, B., Stanifer, M.L., Boulant, S., Bartenschlager, R., Chlanda, P., 2020. Sars-cov-2 structure and replication characterized by *in situ* cryo-electron tomography. Nat. Commun. 11, 5885.

Li, Q., Liu, Q., Li, S., Zuo, X., Zhou, H., Gao, Z., Xia, B., 2025. Golgi-derived extracellular vesicle production induced by sars-cov-2 envelope protein. Apoptosis 30, 197–209.

Li, S., Bu, J., Pan, X., Li, Q., Zuo, X., Xiao, G., Du, J., Zhang, L.K., Xia, B., Gao, Z., 2024. Sars-cov-2 envelope protein-derived extracellular vesicles act as potential media for viral spillover. J. Med. Virol. 96, e29782.

Liu, L., Zhang, L., Hao, X., Wang, Y., Zhang, X., Ge, L., Wang, P., Tian, B., Zhang, M., 2024. Coronavirus envelope protein activates tmed10-mediated unconventional secretion of inflammatory factors. Nat. Commun. 15, 8708.

Minigulov, N., Boranbayev, K., Bekbossynova, A., Gadilgereyeva, B., Filchakova, O., 2024. Structural proteins of human coronaviruses: what makes them different? Front. Cell. Infect. Microbiol. 14, 1458383.

Mohamud, Y., Qu, J., Xue, Y.C., Liu, H., Deng, H., Luo, H., 2019. Calcoco2/ndp52 and sqstm1/p62 differentially regulate coxsackievirus b3 propagation. Cell Death Differ. 26, 1062–1076.

Nieto-Torres, J.L., Verdiá-Báguena, C., Jimenez-Guardeño, J.M., Regla-Nava, J.A., Castaño-Rodriguez, C., Fernandez-Delgado, R., Torres, J., Aguilella, V.M., Enjuanes, L., 2015. Severe acute respiratory syndrome coronavirus e protein transports calcium ions and activates the nlrp3 inflammasome. Virology 485, 330–339.

Otomo, C., Metlagel, Z., Takaesu, G., Otomo, T., 2013. Structure of the human atg12~atg5 conjugate required for lc3 lipidation in autophagy. Nat. Struct. Mol. Biol. 20, 59–66.

Rashid, H.O., Yadav, R.K., Kim, H.R., Chae, H.J., 2015. Er stress: autophagy induction, inhibition and selection. Autophagy 11, 1956–1977.

Sala, C., Ninu, A., Balducci, V., Allegro, G., Montalbano, A., Lulli, M., Boccitto, M.L., Guzzolino, E., Spinelli, V., Arcangeli, A., Sartiani, L., Cerbai, E., 2025. Stable expression of sars-cov-2 envelope viroporin promotes intracellular calcium depletion in human cells: relevance for endoplasmic reticulum stress, cell proliferation, pluripotency and lineage differentiation. Cell Calcium 128, 103032.

Schoeman, D., Fielding, B.C., 2019. Coronavirus envelope protein: current knowledge. Virol. J. 16, 69.

Siu, K.L., Chan, C.P., Kok, K.H., Woo, P.C., Jin, D.Y., 2014. Comparative analysis of the activation of unfolded protein response by spike proteins of severe acute respiratory syndrome coronavirus and human coronavirus hku1. Cell Biosci. 4, 3.

Sučec, I., Xia, B., Somberg, N.H., Wang, Y., Jo, H., Li, S., Perrone, B., Gao, Z., Hong, M., 2025. Ion channel structure and function of the mers coronavirus e protein. Sci. Adv. 11, eadx1788.

Volovik, M.V., Denieva, Z.G., Gifer, P.K., Rakitina, M.A., Batishchev, O.V., 2024. Membrane activity and viroporin assembly for the sars-cov-2 e protein are regulated by cholesterol. Biomolecules 14, 1061.

Wagh, A.R., Sulakshane, P., Glickman, M.H., 2023. Alzheimer's disease-associated mutant ubiquitin (ubb(+1)) is secreted through an autophagosome-like vesicle-mediated unconventional pathway. Biochim. Biophys. Acta, Gene Regul. Mech. 1866, 194936.

Walczak, M., Martens, S., 2013. Dissecting the role of the atg12-atg5-atg16 complex during autophagosome formation. Autophagy 9, 424–425.

Wang, L., Ou, J.H., 2015. Hepatitis c virus and autophagy. Biol. Chem. 396, 1215–1222.

Wang, P., Tian, B., Xiao, K., Ji, W., Li, Z., 2025a. The sars-cov-2 nsp4 t492i mutation promotes double-membrane vesicle formation to facilitate transmission. Virol. Sin. 40, 225–235.

Wang, Q., Peng, Z., Chu, P., Gui, B., Li, Y., Liao, L., Zhu, Z., Ke, F., Wang, Y., He, L., 2025b. Type ii grass carp reovirus utilizes autophagosomes for viroplasm formation and subclinical persistent infection. J. Virol. 99, e0035225.

Williams, J.M., Chen, Y.J., Cho, W.J., Tai, A.W., Tsai, B., 2023. Reticulons promote formation of er-derived double-membrane vesicles that facilitate sars-cov-2 replication. J. Cell Biol. 222, e202203060.

Wolff, G., Limpens, R., Zevenhoven-Dobbe, J.C., Laugks, U., Zheng, S., de Jong, A.W.M., Koning, R.I., Agard, D.A., Grünewald, K., Koster, A.J., Snijder, E.J., Bárcena, M., 2020. A molecular pore spans the double membrane of the coronavirus replication organelle. Science 369, 1395–1398.

Zhai, H., Wang, T., Liu, D., Pan, L., Sun, Y., Qiu, H.J., 2023. Autophagy as a dual-faced host response to viral infections. Front. Cell. Infect. Microbiol. 13, 1289170.

Zhang, Y., Sun, H., Pei, R., Mao, B., Zhao, Z., Li, H., Lin, Y., Lu, K., 2021. The sars-cov-2 protein orf3a inhibits fusion of autophagosomes with lysosomes. Cell Discov. 7, 31.